Inorganic Chemistry

pubs.acs.org/IC Article

Redox-Inactive Metal Ions That Enhance the Nucleophilic Reactivity of an Alkylperoxocopper(II) Complex

Bohee Kim, Seonghan Kim, Takehiro Ohta, and Jaeheung Cho*

Cite This: https://dx.doi.org/10.1021/acs.inorgchem.0c01109 Read Online

ACCESS | Metrics & More | Article Recommendations | Supporting Information

ABSTRACT: The importance of redox-inactive metal ions in modulating the reactivity of redox-active biological systems is a subject of great current interest. In this work, the effect of redox-inactive metal ions (M^{3+} = Sc^{3+}, Y^{3+}, Yb^{3+}, La^{3+}) on the nucleophilic reactivity of a mononuclear ligand-based alkylperoxocopper(II) complex, $[Cu(^{i}Pr_2\text{-tren-}C(CH_3)_2O_2)]^+$ (**1**), was examined. **1** was prepared by the addition of hydrogen peroxide and triethylamine to the solution of $[Cu(^{i}Pr_3\text{-tren})(CH_3CN)]^+$ ($^{i}Pr_3$-tren = tris[2-(isopropylamino)ethyl]amine) via the formation of $[Cu(^{i}Pr_3\text{-tren})(O_2H)]^+$ (**2**) in methanol (CH_3OH) at 30 °C. **1** was characterized using density functional theory (DFT) calculations and spectroscopic methods such as UV−vis, resonance Raman (rR), and electron paramagnetic resonance (EPR). DFT calculations support the electronic structure of **1** with an intermediate geometry between the trigonal-bipyramidal and square-pyramidal geometries, which is consistent with the observed EPR signal exhibiting a signal with $g_\perp$ = 2.03 ($A_\perp$ = 16 G) and $g_\parallel$ = 2.19 ($A_\parallel$ = 158 G). The Cu−O bond stretching frequency of **1** was observed at 507 cm^{-1} for $^{16}O_2$ species (486 cm^{-1} for $^{18}O_2$ species), and its O−O vibrational energy was determined to be 799 cm^{-1} for $^{16}O_2$ species (759 cm^{-1} for $^{18}O_2$ species) by rR spectroscopy. The reactivity of **1** was investigated in oxidative nucleophilic reactions. The positive slope of the Hammett plot (ρ = 2.3(1)) with para-substituted benzaldehydes and the reactivity order with 1°-, 2°-, and 3°-CHO demonstrate well the nucleophilic character of this copper(II) ligand-based alkylperoxo complex. The Lewis acidity of M^{3+} improves the oxidizing ability of **1**. The modulated reactivity of **1** with M^{3+} was revealed to be an opposite trend of the Lewis acidity of M^{3+} in aldehyde deformylation.

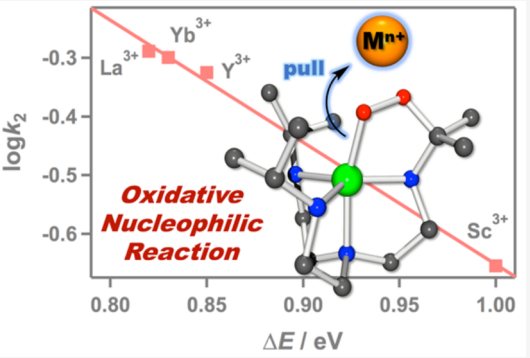

INTRODUCTION

It is regarded that redox-inactive metal ions play a key role in biological and biomimetic processes. In photosystem II, water is oxidized to dioxygen (O_2) by an oxygen-evolving complex (OEC), which is composed of the Mn_4CaO_5 cluster.[1−3] It is suggested that a redox-inactive Ca^{2+} ion plays a role in O−O bond formation to generate O_2 in OEC.[4,5] Elucidation of the role of redox-inactive metal ions has attracted much interest in the past 10 years.[6,7] To investigate the role of redox-inactive metal ions in transition-metal reactive oxygen adducts such as metal−oxo, −peroxo, and −superoxo species, a number of metal−oxygen adducts binding to redox-inactive metal ions have been prepared and characterized in biomimetic chemistry.[8−10] In particular, it has been demonstrated that redox-inactive metal ions acting as Lewis acids affected the various oxidation reactions. Binding of secondary metal ions such as Ca^{2+}, Mg^{2+}, Zn^{2+}, Lu^{3+}, Y^{3+}, Al^{3+}, and Sc^{3+} to high-valent metal−oxo complexes improves the oxidizing power in O-atom transfer as well as electron transfer.[11−15] In addition, catalysts binding redox-inactive metal ions lead to a rise in the catalytic efficiency in sulfoxidation and epoxidation.[16,17] Although the role of secondary metal ions with metal reactive oxygen complexes has been widely explored, the scope of the study is still limited to metal−oxo species. Recently, Nam's group reported the first instance of the modulated reactivity of an iron−peroxo complex with redox-inactive metal ions in electrophilic and nucleophilic reactions.[18]

Ligand-based alkylperoxide binding metal complexes have been proposed as intermediates, which functionalize the aliphatic C−H bond.[19−21] In synthetic chemistry, Suzuki and co-workers have shown the first crystal structures of $[Ni_2(Me\text{-}tpa\text{-}CH_2O_2)_2]^{2+}$ (Scheme 1a)[19] and $[Cu(Me\text{-}tpa\text{-}CH_2O_2)]^+$ (Scheme 1b)[20] through oxidation of the methyl group of the Me_2-tpa ligand. Although well-characterized ligand-based alkylperoxometal complexes were recognized as intermediates in ligand oxidation, the reactivity of the ligand-based alkylperoxometal species toward external substrates has not been revealed. On the other hand, it is well demonstrated that the alkylperoxocopper(II) complexes can conduct electrophilic reactions through O−O bond cleavage, which affords putative

Received: April 16, 2020

Scheme 1. Representations of the Ligand-Based Alkylperoxometal Complexes: X-ray Structures for (a) $[Ni_2(Me\text{-}tpa\text{-}CH_2O_2)_2]^{2+}$ and (b) $[Cu(Me\text{-}tpa\text{-}CH_2O_2)]^+$ and (c) DFT Structure for 1[a]

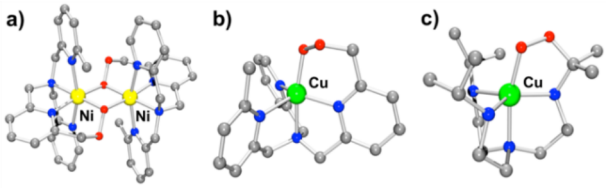

[a]Color code: gray, C; blue, N; red, O, yellow, Ni; green, Cu.

copper(II)−oxyl radical or copper(III)−oxo species.[22,23] Very recently, it was also reported that alkylperoxocopper(II) complexes carry out aldehyde deformylation through cleavage of the Cu−O bond.[24]

Herein, we report the nucleophilic reactivity of a mononuclear alkylperoxocopper(II) complex, $[Cu(^iPr_2\text{-tren-}C(CH_3)_2O_2)]^+$ (**1**; Scheme 1c), toward various aldehydes. Complex **1** is of a ligand-based alkylperoxo moiety through C−H bond activation of one of the isopropyl groups (Scheme S1). Kinetic studies including Hammett analysis and a reactivity order in the oxidation of a series of alkylaldehydes demonstrate the nucleophilic character of **1**. Moreover, the oxidative nucleophilic reactivity of **1** was modulated by the Lewis acidity of redox-inactive metal ions such as Sc^{3+}, Y^{3+}, Yb^{3+}, and La^{3+}.

EXPERIMENTAL SECTION

Materials. All chemicals obtained from Aldrich Chemical Co. were of the best available purity and were used without further purification unless otherwise indicated. The solvents acetonitrile (CH_3CN), methanol (CH_3OH), and diethyl ether (Et_2O) were passed through solvent purification columns (JC Meyer Solvent Systems) prior to use. $H_2{}^{18}O_2$ (95% ^{18}O-enriched and 2.2% $H_2{}^{18}O_2$ in water) was purchased from ICON Services Inc. (Summit, NJ). The tris[2-(isopropylamino)-ethyl]amine ($^iPr_3$-tren) ligand and redox-inactive metal triflates $M(CF_3SO_3)_3$ ($M = Sc^{3+}$, Y^{3+}, Yb^{3+}, La^{3+}) were obtained from Aldrich Chemical Co.

Instrumentation. UV−vis spectra were recorded on a Hewlett-Packard 8454 diode-array spectrophotometer equipped with a UNISOKU scientific instrument for low-temperature experiments or with a circulating water bath. Electrospray ionization mass spectrometry (ESI-MS) spectra were collected on a Waters (Milford, MA) Acquity SQD quadrupole mass instrument by infusing samples directly into the source using a manual method. The spray voltage was set at 2.5 kV and the capillary temperature at 80 °C. Resonance Raman (rR) spectra were obtained using a liquid-nitrogen-cooled charge-coupled detector (CCD-1024×256-OPEN-1LS; Horiba Jobin Yvon, Kyoto, Japan) attached to a 1 m single polychromator (MC-100DG; Ritsu Oyo Kogaku, Saitama, Japan) with a 1200 grooves/mm holographic grating. An excitation wavelength of 405 nm was provided by a diode laser (LM-405-PLR-40-2, Ondax, Inc., Monrovia, CA), with 10 mW power at the sample point. All measurements were performed with a spinning cell at −30 °C. Raman shifts were calibrated with indene, and the accuracy of the peak positions of the Raman bands was ±1 cm^{-1}. Electron paramagnetic resonance (EPR) spectra were obtained on a JEOL JES-FA200 spectrometer. EPR spin quantification was carried out using a spin quantification program, JEOL v 2.8.0. v2 series. The spectral simulation was carried out using a simulation software, JEOL AniSimu/FA, version 2.4.0. Product analysis was performed on a Thermo Fisher Trace 1310 gas chromatograph system equipped with a flame ionization detector.

Generation and Characterization of $[Cu(^iPr_2\text{-tren-}C(CH_3)_2O_2)]^+$ (1). The treatment of $[Cu(^iPr_3\text{-tren})(CH_3CN)](ClO_4)_2$ (1 mM) with 10 equiv of hydrogen peroxide (H_2O_2) in the presence of 4 equiv of triethylamine (TEA) in CH_3OH at 30 °C afforded a green solution. $[Cu(^iPr_2\text{-tren-}C(CH_3)_2{}^{18}O_2)]^+$ (**1**-^{18}O) was prepared by adding 10 equiv of $H_2{}^{18}O_2$ (72 μL, 95% ^{18}O-enriched, 2.2% $H_2{}^{18}O_2$ in water) to a solution containing $[Cu(^iPr_3\text{-tren})(CH_3CN)](ClO_4)_2$ (1 mM) and 4 equiv of TEA in CH_3OH at 30 °C. UV−vis [CH_3OH; λ_{max}, nm (ε, M^{-1} cm^{-1})]: 367 (710), 650 (160), 810 (110) (Figure 1a).

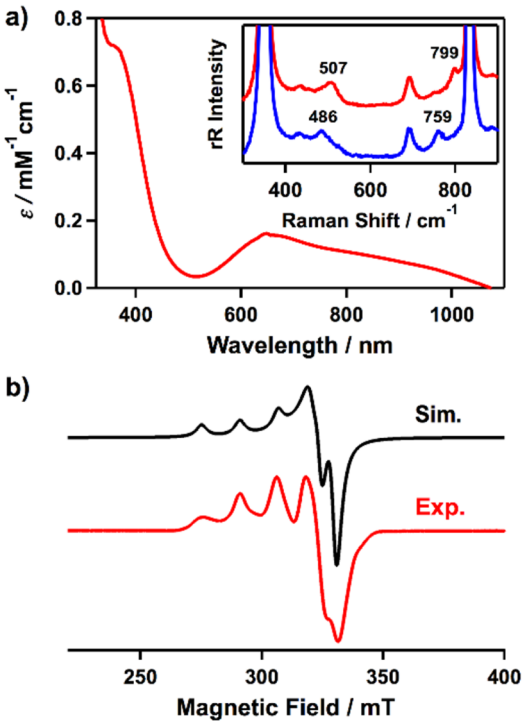

Figure 1. (a) UV−vis spectrum of **1** in CH_3OH at 30 °C. The inset shows the rR spectra of **1** (16 mM) prepared with $H_2{}^{16}O_2$ (red line) and $H_2{}^{18}O_2$ (blue line) in CH_3OH at −30 °C. (b) X-band EPR spectrum (red line) and simulation (black line) of **1** in frozen CH_3OH at 113 K.

Reactivity Studies. All reactions were performed in a 1 cm UV cuvette by monitoring UV−vis spectral changes of the reaction solutions, and rate constants were determined by fitting the changes in absorbance at 380 nm for **1** in the absence and presence of redox-inactive metal ions ($M^{3+} = La^{3+}$, Yb^{3+}, Y^{3+}, Sc^{3+}). Reactions were run at least in triplicate, and the data reported represent the average of these reactions. In situ generated **1** (2 mM) with and without M^{3+} (3 mM) was used in reactivity studies, such as the oxidation of cyclohexylcarboxaldehyde (CCA) in CH_3OH at 30 °C (Figures 2−4). After completion of the reactions, pseudo-first-order fitting of the kinetic data allowed us to determine k_{obs} values. Products, formed in the oxidation of CCA by **1** with and without M^{3+} in CH_3OH at 30 °C, were analyzed by injecting the reaction mixture directly into a gas chromatograph. All peaks of products were identified by comparing the retention times with those of the authentic samples. The products were quantified by comparing their peak areas with that of an internal standard using calibration curves.

Computational Details. Theoretical calculations were performed with density functional theory (DFT)[25] using the *Gaussian 09* package.[26] The B3LYP functional was employed for all geometry optimizations with double-ζ basis set 6-31G* for all atoms.[27] All calculations, including optimizations, were performed in a solvent (methanol) using the CPCM scheme.[28] Optimized geometries were visualized with *Gaussview 6*. The root-mean-square deviation (RMSD) value (0.13 Å) supports the credibility of the DFT calculations, where the RMSD value was previously obtained by comparing the optimized geometry of $[Cu(^iPr_3\text{-tren})(CH_3CN)]^{2+}$

https://dx.doi.org/10.1021/acs.inorgchem.0c01109
Inorg. Chem. XXXX, XXX, XXX−XXX

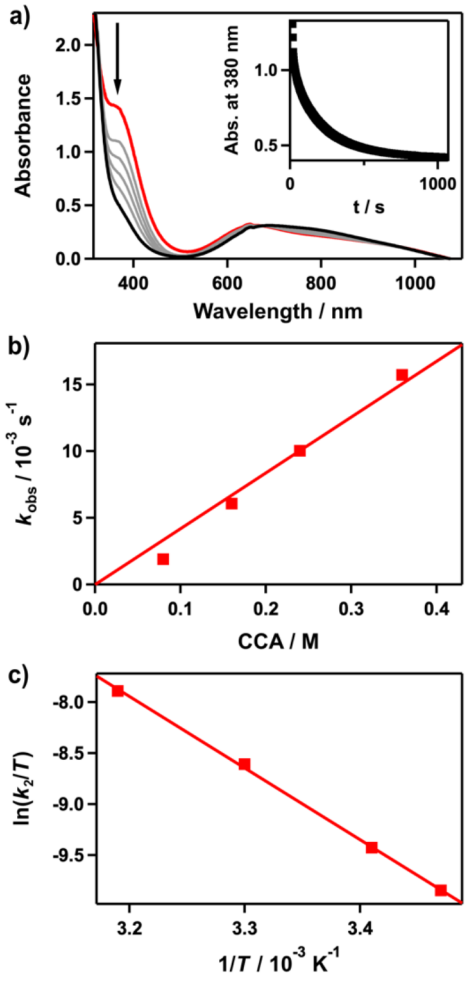

Figure 2. Reactions of **1** with CCA in CH_3OH. (a) UV−vis spectral changes of **1** (2 mM) with 80 equiv of CCA at 30 °C. The inset shows the time course of the absorbance at 380 nm. (b) Plot of k_{obs} against the CCA concentration to determine a second-order rate constant for **1** at 30 °C. (c) Plot of second-order rate constants against $1/T$ to determine the activation parameters.

with the crystal structure of $[Cu(^{i}Pr_3\text{-tren})(CH_3CN)]^{2+}$.[29] Populations were obtained from Mulliken analysis. Molecular orbital compositions and overlap populations between molecular fragments were calculated using *QMForge*.[30] Time-dependent DFT (TD-DFT) calculations were carried out with 150 roots.[31]

RESULTS AND DISCUSSION

Synthesis and Characterization of 1. The alkylperoxocopper(II) complex **1** was generated in the reaction of $[Cu(^{i}Pr_3\text{-tren})(CH_3CN)]^{2+}$ with 10 equiv of H_2O_2 and 4 equiv of TEA in CH_3OH at 30 °C via the formation of $[Cu(^{i}Pr_3\text{-tren})(O_2H)]^{+}$ (**2**; see the Experimental Section and Scheme S1). Very recently, we reported the formation of **2**, which was metastable at −40 °C.[29] Complex **2** decomposes readily to **1** in CH_3OH at 30 °C (see the Experimental Section and Scheme S1).

The green solution of complex **1** exhibited three absorption bands at about λ_{max} = 367 nm (ε = 710 M^{-1} cm^{-1}), 650 nm (ε = 160 M^{-1} cm^{-1}), and 810 nm (ε = 110 M^{-1} cm^{-1}) in the UV−vis spectrum (Figure 1a). The absorption spectrum of **1** is very similar to that of the reported ligand-based alkylperoxocopper(II) complex, $[Cu(Me\text{-}tpa\text{-}CH_2O_2)]^{+}$ (Scheme 1b).[20] The rR spectrum of **1** was observed by using 405 nm excitation in CH_3OH at −30 °C (Figure 1a, inset). **1**-^{16}O exhibited two isotope-sensitive bands at 799 and 507

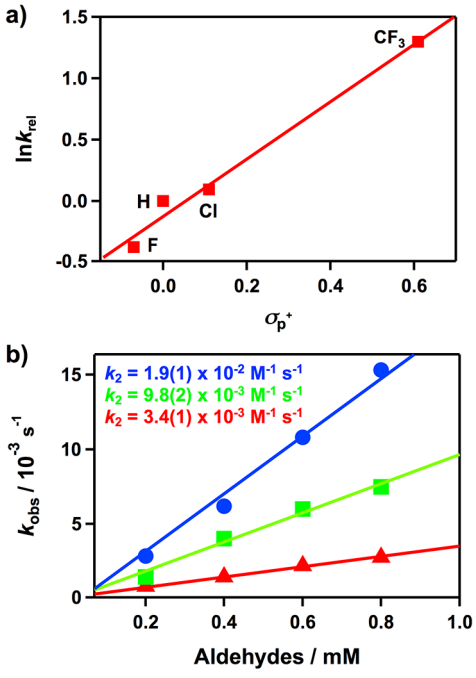

Figure 3. (a) Hammett plot of ln k_{rel} against σ_p^+ of benzaldehyde derivatives in the reaction of **1** with para-substituted benzaldehydes. The k_{rel} values were calculated by dividing k_{obs} of *p*-X-Ph-CHO (X = F, H, Cl, CF_3) by k_{obs} of benzaldehyde in CH_3OH at 30 °C. (b) Second-order rate constants determined in the reactions of **1** with pentanal (1°-CHO; circles), 2-methylbutanal (2°-CHO; squares), and pivalaldehyde (3°-CHO; triangles) in CH_3OH at 30 °C.

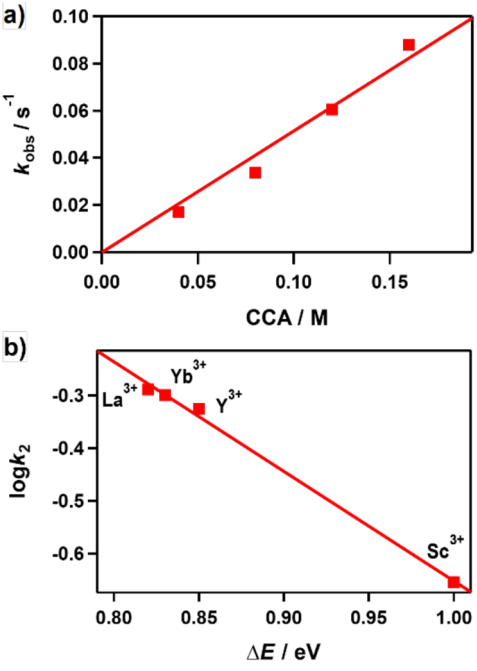

Figure 4. Reactions of **1** in the presence of La^{3+} with CCA in CH_3OH at 30 °C. (a) Plot of k_{obs} against the CCA concentration to determine a second-order rate constant for **1** in the presence of La^{3+}. (b) Plot of log k_2 values of the deformylation reaction with CCA by **1** in the presence of Sc^{3+}, Y^{3+}, Yb^{3+}, and La^{3+}.

https://dx.doi.org/10.1021/acs.inorgchem.0c01109
Inorg. Chem. XXXX, XXX, XXX−XXX

cm^{-1}, which shifted to 759 and 486 cm^{-1} in **1**-^{18}O. The bands at 799 and 507 cm^{-1} can be assigned as O−O and Cu−O stretching vibrations on the basis of $^{16-18}\Delta$ values of 40 and 21 cm^{-1} ($^{16-18}\Delta$(calcd) = 48 and 23 cm^{-1} for a diatomic harmonic oscillator), respectively. These results are comparable to $[Cu(Me\text{-}tpa\text{-}CH_2O_2)]^+$ [(ν(O−O) = 789 and 804 cm^{-1}; ν(Cu−O) = 498 cm^{-1}).[20]

The EPR spectrum of a frozen solution of **1** at 113 K shows a signal with $g_\perp$ = 2.03 ($A_\perp$ = 16 G) and $g_\parallel$ = 2.19 ($A_\parallel$ = 158 G), which indicates an intermediate geometry between the trigonal-bipyramidal and square-pyramidal geometries (Figure 1b).[32,33] The results were further supported by DFT calculations (vide infra). Spin quantification found that the EPR signal corresponds to 93(7)% of the total copper content in the sample (see the Experimental Section).

DFT Calculations. The optimized geometric and electronic structures of **1** were calculated by DFT at the spin-unrestricted B3LYP theory level (see Computational Details). The optimized structure of **1** revealed an intermediate geometry between the trigonal-bipyramidal and square-pyramidal geometries with τ = 0.52, which is similar to that of $[Cu(Me\text{-}tpa\text{-}CH_2O_2)]^+$ (τ = 0.51;[20] Scheme 1b,c and Table S1 and Figure S1),[34] and its axial site is occupied by the ligand-based alkylperoxo group. The calculated O−O bond distance (1.47 Å) showed a similar observation with $[Cu(Me\text{-}tpa\text{-}CH_2O_2)]^+$ (1.47 Å) and Kitajima's alkylperoxocopper(II) complex (1.46 Å).[20,35] TD-DFT calculations exhibited that the electronic transitions of **1** are in agreement with the experimental UV−vis spectrum. The calculated absorption spectrum displayed an intense peak at 385 nm and multiple weak peaks in the range from 550 to 750 nm (Figure S2). The peak at 385 nm indicated a form of ligand-to-metal charge transfer from mixed orbitals among the supporting ligand (25%), alkylperoxide (44%), and d orbitals in Cu (32%) to σ* orbitals between π* orbitals in alkylperoxide (21%) and the d_{z^2} orbital in Cu (68%; Figure S3). The multiple minor weak peaks in the 550−750 nm range are assigned to d−d transitions. The singly occupied molecular orbital (SOMO) for **1** was observed to be combined with the π* orbital in alkylperoxide and d_{z^2} orbitals in Cu. The calculated spin-density distribution of the SOMO indicates that over half a radical belongs to the Cu center and the rest is contained in the alkylperoxide and ligand with a doublet state (Figure S4 and Table S3). Thus, all of the spectroscopic data and DFT calculations clearly support that **1** is assigned as an alkylperoxocopper(II) intermediate between the trigonal-bipyramidal and square-pyramidal geometries.

Reactivity Study of 1. It is well-known that metal−hydroperoxo and −alkylperoxo complexes exhibit electrophilic reactivity through O−O bond cleavage, affording metal−oxyl radical or metal−oxo species. However, the nucleophilic reactivity of Cu^{II}-OOR (R = H, cumyl, and *tert*-butyl) complexes has also been reported in recent years.[24,29] The electrophilic reactivity of **1** was examined with thioanisole and cyclohexadiene. By addition of the substrates to **1** in CH_3OH at 30 °C, **1** remained intact, and only trace amounts of products were detected in the reaction solution (Figure S5).

We also investigated the nucleophilic reaction of **1** with CCA. Upon the addition of 80 equiv of CCA to **1** in CH_3OH at 30 °C, the characteristic absorption bands of **1** decreased with a first-order decay profile (Figure 2a). Product analyses of the reaction solution of **1** with CCA showed cyclohexene (87(10)%) as a major organic product and an iminated formatocopper(II) complex, $[Cu\{N(CH_2CH_2N{=}C(CH_3)_2)(CH_2CH_2NHCH(CH_3)_2)_2\}(CHOO)]^+$ (Figure S6). A second-order rate constant (k_2) for the oxidation of CCA by **1** was obtained to be 5.5(4) × 10^{-2} M^{-1} s^{-1} from a linear correlation of the first-order rate constants against the concentration of CCA (Figure 2b). The activation parameters were determined by the reaction temperature dependence of the k_2 value for the oxidation of CCA with **1** to be $\Delta H^\ddagger$ = 59(1) kJ mol^{-1} and ΔS = −75(2) J mol^{-1} K^{-1} in the range of 233−258 K (Figure 2c). A bimolecular mechanism for the oxidative reaction of **1** with CCA is suggested by the observed negative entropy and second-order kinetics.

In the oxidation reaction of aromatic aldehydes, the nucleophilic reactivity of **1** was further examined. The Hammett plot of the first-order rate constant against σ_p^+ gave a linear correlation in the reaction of **1** and *p*-X-Ph-CHO (X = F, H, Cl, CF_3), affording a ρ value of 2.3(3) (Figure 3a). After the reaction was completed, product analysis revealed the formation of benzoic acid in a quantitative yield (93(5)%). The positive ρ value implicates a nucleophilic character of **1**. The reactivity of **1** was also investigated by using primary (1°-CHO), secondary (2°-CHO), and tertiary (3°-CHO) aldehydes (Figure 3b). The observed reactivity order of 1°-CHO > 2°-CHO > 3°-CHO supports a nucleophilic character for **1**. Plausible mechanisms for aldehyde oxidation by **1** are described in Scheme S2.

Nucleophilic Reaction of 1 in the Presence of Redox-Inactive Metal Ions. Interestingly, the nucleophilic reactivity of **1** was modulated by the addition of redox-inactive metal ions to the solution of **1**. Upon the addition of 1.5 equiv of La^{3+} to the solution of **1** with CCA, the oxidative reaction was facilitated (Figure S7). Kinetic studies of **1** in the presence of La^{3+} with CCA exhibited a pseudo-first-order reaction profile and the first-order rate constants increased proportionally with the CCA concentration (Figure 4a). Product analysis revealed the formation of cyclohexene (75(2)%) in the reaction solution. The nucleophilic character of **1** in the existence of La^{3+} was also explored in the reaction of *p*-X-Ph-CHO (X = OCH, CH_3, F, H, Cl). The obtained positive ρ value (2.3(1)) indicates that **1** in the presence of La^{3+} has a nucleophilic character (Figure S8). Benzoic acid was obtained in 90(10)% yield from the reaction solution of **1** with La^{3+} and benzaldehyde in CH_3OH. A series of redox-inactive metal ions (M^{3+} = Sc^{3+}, Y^{3+}, Yb^{3+}, La^{3+}) were adopted to investigate the effect of Lewis acidity in the nucleophilic reaction with **1** and CCA (Table S4 and Figure S9). The observed reactivity order is Sc^{3+} < Y^{3+} < Yb^{3+} < La^{3+}, which corresponds to an opposite trend of Lewis acidity of M^{3+} (Figure 4b).[36] Strong Lewis acidity of M^{3+} would cause the withdrawal of electron density from the alkylperoxo moiety, resulting in a decrease of the nucleophilicity of **1** compared to the reaction with weak Lewis acidity of M^{3+}.

Plausible Mechanisms. On the basis of kinetic studies of **1**, the proposed mechanisms for the aldehyde oxidation by **1** with and without Lewis acids are shown in Scheme 2. In the absence of Lewis acids, aldehyde oxidation by **1** would be initiated by the nucleophilic attack of the proximal O atom of the alkylperoxo moiety in **1** to the C atom of the C═O group in aldehydes through Cu−O bond cleavage. Then, O−O bond cleavage of the peroxyhemiacetal-like intermediate produces the products. A similar mechanism has been proposed in the nucleophilic oxidative reaction of the alkylperoxocopper(II) complex.[24] Very recently, Tolman's group demonstrated an alternative pathway for the nucleophilic reaction of copper-

https://dx.doi.org/10.1021/acs.inorgchem.0c01109
Inorg. Chem. XXXX, XXX, XXX−XXX

Scheme 2. Proposed Mechanism for the Reaction of 1 and Aldehydes in the Absence (blue) and Presence (red) of Redox-Inactive Metal Ions (M^{3+})

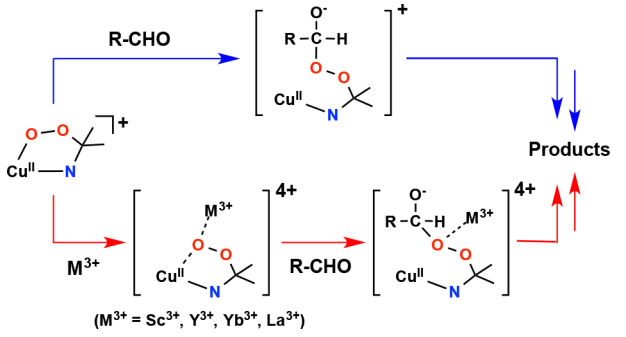

(II)−superoxo species in the presence of water via the formation of a copper(II)−enolate complex, which was generated by deprotonation of α-C−H of the aldehyde with the copper intermediate.[37] We added a proton to **1** to figure out the ability of protonation in **1**. However, **1** remained intact without exhibiting any UV−vis spectral changes upon the addition of $H(CF_3SO_3)$ to the solution of **1**. In addition, any difference of reactivity in the absence and presence of H^+ in the reaction with CCA was not observed. From these results, we may rule out the reaction pathway including enolate species from deprotonation of the aldehyde by **1**.

On the other hand, aldehyde oxidation by **1** in the presence of Lewis acids easily takes place via a second metal-assisted Cu−O bond cleavage compared to that in the absence of Lewis acids. Redox-inactive metal ions facilitate ring cleavage through withdrawal of the electron density of the Cu−O bond, where the nucleophilicity of **1** is increased after Cu−O bond cleavage. Then, the various Lewis acids bound to the proximal O atom of the alkylperoxo moiety pull the electron density from the alkylperoxo moiety to different degrees, modulating the degree of nucleophilic character of the alkylperoxo group in its attack on the C of aldehydes and bringing about a reactivity order with an opposite trend of the Lewis acidity (Figure 4b). DFT calculations are ongoing to investigate the detailed mechanism.

CONCLUSIONS

We have successfully prepared the mononuclear alkylperoxocopper(II) complex **1**, derived from the reaction of the copper(II) precursor complex with H_2O_2 and TEA via the formation of a hydroperoxocopper(II) intermediate. Complex **1** exhibits characteristic features for the ligand-based alkylperoxocopper(II) complex in UV−vis, rR, and EPR analyses. These spectroscopic data show **1** is of an intermediate geometry between the trigonal-bipyramidal and square-pyramidal geometries, which is well matched with theoretical calculations. **1** is capable of performing aldehyde oxidation reactions including aldehyde deformylation. Importantly, the nucleophilic reactivity, which was evidenced by a positive Hammett ρ value in the benzaldehyde oxidation, was enhanced by the addition of redox-inactive metal ions (M^{3+} = La^{3+}, Yb^{3+}, Y^{3+}, Sc^{3+}). A good correlation between the reaction rates of **1** in the aldehyde deformylation and the Lewis acidity of M^{3+} was observed in the order of La^{3+} > Yb^{3+} > Y^{3+} > Sc^{3+}. Thus, the oxidative nucleophilic reactivity of **1** can be modulated by the redox-inactive metal ions.

ASSOCIATED CONTENT

Supporting Information

The Supporting Information is available free of charge at https://pubs.acs.org/doi/10.1021/acs.inorgchem.0c01109.

Tables S1−S4, Schemes S1 and S2, and Figures S1−S9 (PDF)

AUTHOR INFORMATION

Corresponding Author

Jaeheung Cho − *Department of Emerging Materials Science, DGIST, Daegu 42988, Korea;* orcid.org/0000-0002-2712-4295; Email: jaeheung@dgist.ac.kr

Authors

Bohee Kim − *Department of Emerging Materials Science, DGIST, Daegu 42988, Korea*

Seonghan Kim − *Department of Emerging Materials Science, DGIST, Daegu 42988, Korea*

Takehiro Ohta − *Picobiology Institute, Graduate School of Life Science, University of Hyogo, Hyogo 679-5148, Japan;* orcid.org/0000-0003-4140-5293

Complete contact information is available at: https://pubs.acs.org/10.1021/acs.inorgchem.0c01109

Author Contributions

B.K. and J.C. conceived and designed the experiments; B.K., S.K., and T.O. performed the experiments; B.K., S.K., and J.C. analyzed the data; B.K., S.K., and J.C. cowrote the paper.

Notes

The authors declare no competing financial interest.

ACKNOWLEDGMENTS

This work was supported by the NRF funded by the Ministry of Science, ICT and Future Planning (Grants 2019R1A2C2086249, 2018R1A5A1025511, and 2016M3D3A01913243 to J.C.) of Korea and the Ministry of Education, Culture, Sports, Science and Technology of Japan through the "Strategic Young Researcher Overseas Visits Program for Accelerating Brain Circulation" (to T.O.).

DEDICATION

This paper is dedicated to the memory of Professor Takashi Ogura (deceased July 23, 2017).

REFERENCES

(1) Dau, H.; Haumann, M. The manganese complex of photosystem II in its reaction cycle - Basic framework and possible realization at the atomic level. *Coord. Chem. Rev.* **2008**, *252*, 273−295.

(2) Renger, G. Mechanism of light induced water splitting in photosystem II of oxygen evolving photosynthetic organisms. *Biochim. Biophys. Acta, Bioenerg.* **2012**, *1817*, 1164−1176.

(3) Umena, Y.; Kawakami, K.; Shen, J.-R.; Kamiya, N. Crystal structure of oxygen-evolving photosystem II at a resolution of 1.9 Å. *Nature* **2011**, *473*, 55−60.

(4) Yachandra, V. K.; Yano, J. Calcium in the oxygen-evolving complex: Structural and mechanistic role determined by X-ray spectroscopy. *J. Photochem. Photobiol., B* **2011**, *104*, 51−59.

(5) Lee, C.-I.; Lakshmi, K. V.; Brudvig, G. W. Probing the functional role of Ca^{2+} in the oxygen-evolving complex of photosystem II by metal ion inhibition. *Biochemistry* **2007**, *46*, 3211−3223.

(6) Liu, Y.; Lau, T.-C. Activation of metal oxo and nitrido complexes by Lewis acids. *J. Am. Chem. Soc.* **2019**, *141*, 3755−3766.

https://dx.doi.org/10.1021/acs.inorgchem.0c01109
Inorg. Chem. XXXX, XXX, XXX−XXX

(7) Fukuzumi, S.; Ohkubo, K.; Lee, Y.-M.; Nam, W. Lewis acid coupled electron transfer of metal−oxygen intermediates. *Chem. - Eur. J.* **2015**, *21*, 17548−17559.
(8) Lee, Y. M.; Bang, S.; Yoon, H.; Bae, S. H.; Hong, S.; Cho, K.- B.; Sarangi, R.; Fukuzumi, S.; Nam, W. Tuning the redox properties of a nonheme iron(III)-peroxo complex binding redox-inactive zinc ions by water molecules. *Chem. - Eur. J.* **2015**, *21*, 10676−10680.
(9) Lee, Y.-M.; Bang, S.; Kim, Y. M.; Cho, J.; Hong, S.; Nomura, T.; Ogura, T.; Troeppner, O.; Ivanovic-Burmazovic, I.; Sarangi, R.; Fukuzumi, S.; Nam, W. A mononuclear nonheme iron(III)−peroxo complex binding redox-inactive metal ions. *Chem. Sci.* **2013**, *4*, 3917−3923.
(10) Park, Y. J.; Ziller, J. W.; Borovik, A. S. The effects of redox inactive metal ions on the activation of dioxygen: Isolation and characterization of a heterobimetallic complex containing a Mn^{III}−(μ-OH)−Ca^{II} core. *J. Am. Chem. Soc.* **2011**, *133*, 9258−9261.
(11) Leeladee, P.; Baglia, R. A.; Prokop, K. A.; Latifi, R.; de Visser, S. P.; Goldberg, D. P. Valence tautomerism in a high-valent manganese−oxo porphyrinoid complex induced by a Lewis acid. *J. Am. Chem. Soc.* **2012**, *134*, 10397−10400.
(12) Baglia, R. A.; Krest, C. M.; Yang, T.; Leeladee, P.; Goldberg, D. P. High-valent manganese-oxo valence tautomers and the influence of Lewis/Brönsted acids on C-H bond cleavage. *Inorg. Chem.* **2016**, *55*, 10800−10809.
(13) Hong, S.; Pfaff, F. F.; Kwon, E.; Wang, Y.; Seo, M. S.; Bill, E.; Ray, K.; Nam, W. Spectroscopic capture and reactivity of a low-spin cobalt(IV)-oxo complex stabilized by binding redox-inactive metal ions. *Angew. Chem., Int. Ed.* **2014**, *53*, 10403−10407.
(14) Hong, S.; Lee, Y. M.; Sankaralingam, M.; Vardhaman, A. K.; Park, Y. J.; Cho, K. B.; Ogura, T.; Sarangi, R.; Fukuzumi, S.; Nam, W. A manganese(V)-oxo complex: Synthesis by dioxygen activation and enhancement of its oxidizing power by binding scandium ion. *J. Am. Chem. Soc.* **2016**, *138*, 8523−8532.
(15) Chen, J.; Lee, Y.-M.; Davis, K. M.; Wu, X.; Seo, M. S.; Cho, K.-B.; Yoon, H.; Park, Y. J.; Fukuzumi, S.; Pushkar, Y. N.; Nam, W. A mononuclear non-heme manganese(IV)−oxo complex binding redox-inactive metal ions. *J. Am. Chem. Soc.* **2013**, *135*, 6388−6391.
(16) Dong, L.; Wang, Y. J.; Lv, Y. Z.; Chen, Z. Q.; Mei, F. M.; Xiong, H.; Yin, G. C. Lewis-acid-promoted stoichiometric and catalytic oxidations by manganese complexes having cross-bridged cyclam ligand: A comprehensive study. *Inorg. Chem.* **2013**, *52*, 5418−5427.
(17) Nodzewska, A.; Watkinson, M. Remarkable increase in the rate of the catalytic epoxidation of electron deficient styrenes through the addition of $Sc(OTf)_3$ to the MnTMTACN catalyst. *Chem. Commun.* **2018**, *54*, 1461−1464.
(18) Bae, S. H.; Lee, Y.-M.; Fukuzumi, S.; Nam, W. Fine control of the redox reactivity of a nonheme iron(III)-peroxo complex by binding redox-inactive metal ions. *Angew. Chem., Int. Ed.* **2017**, *56*, 801−805.
(19) Cho, J.; Furutachi, H.; Fujinami, S.; Suzuki, M. A bis(m-alkylperoxo)dinickel(II) complex as a reaction intermediate for the oxidation of the methyl groups of the Me_2-tpa ligand to carboxylate and alkoxide ligands. *Angew. Chem., Int. Ed.* **2004**, *43*, 3300−3303.
(20) Mizuno, M.; Honda, K.; Cho, J.; Furutachi, H.; Tosha, T.; Matsumoto, T.; Fujinami, S.; Kitagawa, T.; Suzuki, M. A mononuclear alkylperoxocopper(II) complex as a reaction intermediate in the oxidation of the methyl group of the supporting ligand. *Angew. Chem., Int. Ed.* **2006**, *45*, 6911−6914.
(21) Halfen, J. A.; Young, V. G.; Tolman, W. B. An unusual ligand oxidation by a (μ-η^2:η^2-Peroxo)dicopper compound: 1° > 3° C−H bond selectivity and a novel bis(μ-alkylperoxo)dicopper intermediate. *Inorg. Chem.* **1998**, *37*, 2102−2103.
(22) Sanyal, I.; Ghosh, P.; Karlin, K. D. Mononuclear copper(I1)-acylperoxo complexes. *Inorg. Chem.* **1995**, *34*, 3050−3056.
(23) Tano, T.; Ertem, M. Z.; Yamaguchi, S.; Kunishita, A.; Sugimoto, H.; Fujieda, N.; Ogura, T.; Cramer, C. J.; Itoh, S. Reactivity of copper(II)-alkylperoxo complexes. *Dalton Trans.* **2011**, *40*, 10326−10336.
(24) Kim, B.; Jeong, D.; Cho, J. Nucleophilic reactivity of copper(II)-alkylperoxo complexes. *Chem. Commun.* **2017**, *53*, 9328−9331.
(25) Kohn, W.; Sham, L. J. Self-consistent equations including exchange and correlation effects. *Phys. Rev.* **1965**, *140*, A1133−A1138.
(26) Frisch, M. J.; Trucks, G. W.; Schlegel, H. B.; Scuseria, G. E.; Robb, M. A.; Cheeseman, J. R.; Scalmani, G.; Barone, V.; Mennucci, B.; Petersson, G. A.; Nakatsuji, H.; Caricato, M.; Li, X.; Hratchian, H. P.; Izmaylov, A. F.; Bloino, J.; Zheng, G.; Sonnenberg, J. L.; Hada, M.; Ehara, M.; Toyota, K.; Fukuda, R.; Hasegawa, J.; Ishida, M.; Nakajima, T.; Honda, Y.; Kitao, O.; Nakai, H.; Vreven, T.; Montgomery, J. A., Jr.; Peralta, J. E.; Ogliaro, F.; Bearpark, M.; Heyd, J. J.; Brothers, E.; Kudin, K. N.; Staroverov, V. N.; Kobayashi, R.; Normand, J.; Raghavachari, K.; Rendell, A.; Burant, J. C.; Iyengar, S. S.; Tomasi, J.; Cossi, M.; Rega, N.; Millam, J. M.; Klene, M.; Knox, J. E.; Cross, J. B.; Bakken, V.; Adamo, C.; Jaramillo, J.; Gomperts, R.; Stratmann, R. E.; Yazyev, O.; Austin, A. J.; Cammi, R.; Pomelli, C.; Ochterski, J. W.; Martin, R. L.; Morokuma, K.; Zakrzewski, V. G.; Voth, G. A.; Salvador, P.; Dannenberg, J. J.; Dapprich, S.; Daniels, A. D.; Farkas, Ö.; Foresman, J. B.; Ortiz, J. V.; Cioslowski, J.; Fox, D. J. *Gaussian 09*, revision D.01; Gaussian, Inc.: Wallingford, CT, 2009.
(27) Becke, A. D. Density-functional thermochemistry. III. The role of exact exchange. *J. Chem. Phys.* **1993**, *98*, 5648−5652.
(28) Cossi, M.; Rega, N.; Scalmani, G.; Barone, V. J. Energies, structures, and electronic properties of molecules in solution with the C-PCM solvation model. *J. Comput. Chem.* **2003**, *24*, 669−681.
(29) Kim, B.; Jeong, D.; Ohta, T.; Cho, J. Nucleophilic reactivity of a copper(II)-hydroperoxo complex. *Commun. Chem.* **2019**, *2*, 81.
(30) Tenderholt, A. *Pyspline and QMForge*; Stanford University Press: Stanford, CA, 2007.
(31) Runge, E.; Gross, E. K. U. Density-functional theory for time-dependent systems. *Phys. Rev. Lett.* **1984**, *52*, 997−1000.
(32) Korkmaz, S. A.; Karadağ, A.; Yerli, Y.; Soylu, M. S. Synthesis and characterization of new heterometallic cyanido complexes based on $[Co(CN)_6]^{3-}$ building blocks: Crystal structure of $[Cu_2(N\text{-bishydeten})_2Co(CN)_6]\bullet 3H_2O$ having a strong antiferromagnetic exchange. *New J. Chem.* **2014**, *38*, 5402−5410.
(33) Matyuska, F.; May, N. V.; Benyei, A.; Gajda, T. Control of structure, stability and catechol oxidase activity of copper(II) complexes by the denticity of tripodal platforms. *New J. Chem.* **2017**, *41*, 11647−11660.
(34) τ is calculated by $\tau = (\beta - \alpha)/60$, where the two greatest valence angles of the metal center are defined as α and β. When the τ value is close to 0, the complex reveals square-pyramidal geometry, and when it is close to 1, the complex exhibits trigonal-bipyramidal geometry. See: Lee, S. C.; Holm, R. H. Synthesis and characterization of an asymmetric bridged assembly containing the unsupported [Fe^{III}-OCu^{II}] bridge: An analog of the binuclear site in oxidized cytochrome c oxidase. *J. Am. Chem. Soc.* **1993**, *115*, 11789−11798.
(35) Kitajima, N.; Katayama, T.; Fujisawa, K.; Iwata, Y.; Morooka, Y. Synthesis, molecular structure, and reactivity of (alkylperoxo)copper-(II) complex. *J. Am. Chem. Soc.* **1993**, *115*, 7872−7873.
(36) Fukuzumi, S.; Ohkubo, K. Quantitative evaluation of Lewis acidity of metal ions derived from the g values of ESR spectra of superoxide: Metal ion complexes in relation to the promoting effects in electron transfer reactions. *Chem. - Eur. J.* **2000**, *6*, 4532−4535.
(37) Bailey, W. D.; Gagnon, N. L.; Elwell, C. E.; Cramblitt, A. C.; Bouchey, C. J.; Tolman, W. B. Revisiting the nucleophilic reactivity of an anionic copper-superoxide complex. *Inorg. Chem.* **2019**, *58*, 4706−4711.

https://dx.doi.org/10.1021/acs.inorgchem.0c01109
Inorg. Chem. XXXX, XXX, XXX−XXX